Assessment of the effect of air pollution controls on trends in shortwave radiation over the United States from 1995 through 2010 from multiple observation networks

Chuen-Meei Gan[1], Jonathan Pleim[1], Rohit Mathur[1], Christian Hogrefe[1], Charles N. Long[2], Jia Xing[1], Shawn Roselle[1] and Chao Wei[1]

(1) Atmospheric Modeling and Analysis Division, National Exposure Research Laboratory, US Environmental Protection Agency, Research Triangle Park, North Carolina, USA

(2) Climate Physics Group, Pacific Northwest National Laboratory, Richland, Washington, USA

Corresponding author: Chuen-Meei Gan, AMAD, NERL, US EPA (chuenmeei@gmail.com, Gan.Meei@epa.gov)

Abstract

Long term datasets of all-sky and clear-sky downwelling shortwave (SW) radiation, cloud cover fraction, and aerosol optical depth (AOD) are analyzed together with surface concentrations from several networks (e.g. SURFRAD, CASTNET, IMPROVE and ARM) in the United States (US). Seven states with varying climatology are selected to better understand the effects of aerosols and clouds on SW radiation. This analysis aims to assess the effects of reductions in anthropogenic aerosol burden resulting from substantial reductions in emissions of sulfur dioxide (SO_2) and nitrogen oxides (NO_x) over the past 16 years across the US on trends in SW radiation. The SO_2 and NO_x emission data show decreasing trends from 1995 to 2010 which indirectly validates the effects of the Clean Air Act (CAA) in the US. Meanwhile, the total column AOD and surface total $PM_{2.5}$ observations also show decreasing trends in the eastern US but slightly increasing trends in the western US. Moreover, measured surface concentrations of several other pollutants (i.e. SO_2, SO_4 and NO_x) have the similar behavior as the AOD and total $PM_{2.5}$. Analysis of the observed data shows strong increasing trends in all-sky downwelling SW radiation with decreasing trends in cloud cover. However, since observations of both all-sky direct and diffuse SW radiation are increasing, there may be

other factors contributing to the radiation trends in addition to the decreasing trends in overall cloud cover. To investigate the role of direct radiative effects of aerosols, clear-sky downwelling radiation is analyzed so that cloud effects are eliminated. However, similar increasing trends in clear-sky total and diffuse SW radiation are observed. While significantly decreasing trends in AOD and surface $PM_{2.5}$ concentrations along with increasing SW radiation (both all-sky and clear-sky) in the eastern US during 1995-2010 imply the occurrence of direct aerosol mediated "brightening", the increasing trends of both all-sky and clear sky diffuse SW radiation contradicts this conclusion since diffuse radiation would be expected to decrease as aerosols direct effects decrease and cloud cover decreases. After investigating several confounding factors, the increasing trend in clear-sky diffuse SW may be due to more high-level cirrus from increasing air traffic over the US. The clear-sky radiation observations in the western US also show indications of "brightening" even though the AOD, $PM_{2.5}$ and surface concentration do not vary drastically. This outcome is not unexpected because the CAA controls were mainly aimed at reducing air pollutant emissions in the eastern US and air pollutant levels in the western US are much lower since the beginning. This suggests other factors affect the "brightening" especially in the western US.

1 Introduction

Solar radiation incident at the surface of the Earth is a key regulator of climate and the primary energy source for life. Several studies in the past (Ohmura and Lang, 1989; Gilgen et al., 1998; Stanhill and Cohen, 2001; Liepert, 2002; Wild et al., 2004; Wild, 2009) have shown evidence of "global dimming" which was described as a widespread decrease of downwelling solar radiation from the early 1960s up to the late 1980s. However, starting during the 1990s, this trend reversed with some regions such as Europe and North America now experiencing "brightening" (Wild et al., 2005; Wild et al., 2009; Pinker et al., 2005; Dutton et al., 2006; Long et al, 2009) possibly due to the air pollution controls. In particular, Wild et al. (2009) and Long et al. (2009) have demonstrated the "brightening" trend with surface radiation measurements (e.g. Baseline Surface Radiation Network (BSRN), Surface Radiation Budget Network (SURFRAD) and Atmospheric Radiation Measurement (ARM)) in Europe and the United States (US). Wild et al. (2009) argued that the "global brightening" was tied to the aerosol loading while Long et al. (2009) attributed this phenomenon to decreasing cloudiness which may or may not be associated with aerosols. Therefore, this study is extended to evaluate the possible causes of the “brightening” in US with more surface measurements.

It is possible that the changes in surface solar radiation are tied to changes in the emissions of aerosols and aerosol precursors, as well as trends in cloud cover. In particular, the reductions of sulfur dioxide (SO_2) and nitrogen oxides (NO_x) emissions have a potential to change anthropogenic aerosol loading which may be associated with trends in regional radiation budgets over the past 16 years. In order to have a better understanding of the aerosol effects and radiation trends, this study employs several observation networks such as SURFRAD, ARM, CASTNET (Clean Air Status and Trend Network) and IMPROVE (Interagency Monitoring of Protection Visual Environments) across the US from 1995 to 2010.

Section 2 gives an overview of each network together with their measurements, instruments, and uncertainties. The methodologies that are applied to each dataset are also discussed. In Section 3, the results from the analyses of these datasets are presented. In this section, the effect of the reduction of SO_2 and NO_x emissions on the radiation budget is assessed by using AOD and surface concentration measurements. In addition, the downwelling SW radiation and cloud cover observations are evaluated to further investigate the aerosol effect. Finally, Section 4 summarizes the findings and conclusions from our analyses.

2 Data and Methodology

2.1 Surface Radiation Budget Network (SURFRAD)

Data from several sources are used in this study. The first dataset is from SURFRAD that includes seven sites that examine different climates throughout the US in Illinois, Montana, Mississippi, Colorado, Pennsylvania, Nevada and South Dakota and is maintained by the National Oceanic and Atmospheric Administration (NOAA). However, the data from South Dakota is not used in this study as the measurements commenced only in 2003. These sites Bondville (BON), Table Mountain (TBL), Goodwin Creek (GWN), Desert Rock (DRA), Fort Peck (FPK), and Penn State (PSU) have been operated for more than a decade. Additional details on each site such as name, operation year and location can be found in Table 1 and Figure 1. Note that even though measurements still continue to the present, in this study we use data collected at the locations through calendar year 2010.

The SURFRAD network not only provides measurements of radiation but also AOD, cloud cover fraction and a variety of meteorological parameters. In this study, we mainly focus on all-sky and clear-sky downwelling SW radiation, AOD and cloud cover fraction. This network measures the direct and diffuse SW radiation with an Eppley Normal Incidence Pyrheliometer (NIP) and shaded Eppley Black and White (B&W), respectively to produce all-sky SW radiation. If the solar tracker does not work properly, a Spectrolab model SR-75 pyranometer is used to measure the all-sky SW radiation. The AOD data is derived based on the measurement of the five spectral SW channels from a Multi Filter Rotating Shadowband Radiometer (MFRSR). In addition, another valuable product, the cloud cover for an effective 160^{o} field of view (FOV) is also derived based on the analysis of surface measurements of total and diffuse downwelling SW radiation (Long et al., 2006). Additional detail on the SURFRAD instruments and measurement techniques can be found in Augustine et al., (2000, 2005 and 2008).

All SURFRAD broadband radiation measurements have a temporal resolution of 3-min averages of 1-s samples up through December 31, 2008, and thereafter are produced as 1-minute averages. However, the resolution of the AOD data varies depending on the raw measurement of the MFRSR as the AOD measurements are not made when clouds interfere with the direct solar beam. In other words, the temporal resolution for AOD is 3-min under clear-sky condition. Thus, there are not always coincident AOD and SW measurements. Also, note that only AOD at 500 nm wavelength is used in this study.

In order to keep the radiation measurements as continuous as possible, quality assurance practices are applied; for instance, exchanging instruments with newly calibrated units annually. The QCRad methodology of Long and Shi (2008) is applied to the radiation data to ensure the data quality is within acceptable range. According to this method, the realistic limits for examining unusual measurements are characterized based on the climatological analyses of radiation observations, particularly from the ARM projects. To produce continuous clear-sky estimates and infer bulk cloud properties from radiation observations, the Radiative Flux Analysis (RFA) is applied after the quality testing. The RFA tool is a series of codes developed to examine the time series of the broadband radiation measurements and detect periods of clear (i.e. cloudless) skies, then use the detected clear-sky data to fit appropriate functions, interpolate the fit coefficients across cloudy periods and thus produce continuous clear-sky radiation estimates. The resultant measured and clear-sky data are then used to infer various atmospheric and cloud microphysical properties, including daylight fractional sky cover for an effective field of view of 160 degrees, effective cloudy sky SW transmissivity calculated as the ratio of the total downwelling SW over the corresponding clear-sky total SW, and visible optical depth for overcast periods. Details of the methodology of these algorithms are available in a series of studies by Long and co-authors (Long and Ackerman 2000, Barnard et al. 2004, Long et al. 2006, Long and Turner 2008, and Barnard et al. 2008).

In this study, the final products which are used in the comparisons are the annual averages. For the radiation data, the averages are estimated based on the approach of Long et al. (2009) which not only reduces the effects of unavailable data (e.g. missing or bad) but also helps to avoid the practice of "filling in" for unavailable data. First, the data are sorted into 15-min bins across each 24-h day (i.e. 96 bins across the day). Then the data within each 15-min bin are averaged to obtain an annual average diurnal cycle (i.e. averaging 365 diurnal cycles). For example, all data for the year 1998 are binned at 15-min resolution to calculate an annual 1998 average diurnal cycle. Next, this annual average diurnal cycle is averaged across the 96 15-min bins to produce the final annual average value. This approach is applied to each year for the data at each SURFRAD and ARM site. We also required data completeness of 80% or greater for each individual year to minimize any artificial effect on inferred seasonal variations and trends. This criterion was met for each year at all sites for the time periods listed in Table 1.

The second measurement that is used in this study is the cloud-free (cloud screened) AOD, which is only available since 1997. The detail of the calibration method, the AOD calculation and the cloud screening method can be found in Harrison et al. (1994) and Augustine et al. (2008). To have the most realistic comparison of AOD with SW radiation trends, we only used AOD measurements that have been cloud screened. However, this cloud screening is different from the Long and Ackerman (2000) clear-sky identification (CSI) method as the CSI method is intended to identify times of hemispherically cloud-free skies, whereas AOD retrievals only require that the path between the instrument and the sun be cloud-free. Thus the Long and Ackerman CSI is much more restrictive than the AOD cloud screening.

To guarantee the quality of the AOD data, Augustine et al. (2008) had compared the measurements at Bondville and Sioux Falls with collocated AERONET sites and showed good agreement in phase and amplitude at both sites (e.g. The coefficient of determination (R^2) values of 0.89 for Bondville and 0.91 for Sioux Falls). Note that greater absolute differences occurred in summer, which is expected as the AOD values are highest during that time of year. The data can be found at http://www.srrb.noaa.gov/surfrad/index.html.

2.2 Atmospheric Radiation Measurement (ARM)

The ARM Climate Research Facility is maintained by the Department of Energy (DOE) and is a multi-platform scientific user facility that supports research of the uncertainties of climate models, particularly the effects of clouds and aerosols. It has three permanent fixed research facilities (i.e. the Southern Great Plains (SGP) and the North Slope of Alaska (NSA) in the U.S., and the Tropical Western Pacific (TWP)) which are designed to obtain data for studying the effects of aerosols, precipitation, surface radiation and clouds on global climate change. ARM also includes additional fixed and mobile sites that are under development to extend the research area in a diverse way.

In this study, we are focusing on the surface radiation data from the SGP site. This facility has multiple radiation measurement systems in the same area. These radiation systems include an Eppley NIP, Precision Spectral Pyranometers (PSP) and shaded Model 8-48 B&W for the SW radiation measurements. For the observations of downwelling direct, diffuse and all-sky SW, the approximated uncertainties are 3% or 4 W/m^2, 6% or 20 W/m^2 and 6% or 10 W/m^2, respectively (Stoffel, 2005). To guarantee the best possible continuous data, the instruments' performance is verified daily (Peppler et al., 2008).

The SW radiation data that is used in this study is the ARM Value Added Product (VAP) called the Flux Analysis (FA) data. More information is available at http://science.arm.gov/vaps/swflux.stm. This dataset is generated by the RFA algorithm (Long and Ackerman, 2000; Long and Gaustad, 2004), which is applied to the ARM data from the SGP network of broadband SW radiometer sites. This is the same algorithm that is applied to the SURFRAD SW radiation dataset (see Section 2.1 for detail). In addition, this dataset is quality tested by the QCRad methodology (Long and Shi, 2008) and its annual average is obtained by the same methodology as described in Section 2.1.

2.3 Clean Air Status and Trends Network (CASTNET)

The Clean Air Status and Trends Network (CASTNET) was established under the 1990 Clean Air Act (CAA) Amendments and has continued and expanded the National Dry Deposition Network, which began in 1987. It is a national, long-term environmental monitoring program operated by the Environmental Protection Agency (EPA) and the National Park Service. It is designed to provide data for evaluating trends in air quality, atmospheric deposition and ecological effects that result from air pollutant emission reductions. Currently, this network operates approximately 84 monitoring sites through the contiguous US, Alaska and Canada. However, for this study, we are only interested in those sites which are in the vicinity of SURFRAD and ARM sites. The information on the selected CASTNET sites that are used in this study can be found in Table 1 and Figure 1. CASTNET focuses on measurements of concentrations of sulfur and nitrogen species and ozone. Concentration measurements for all species except for ozone are made as weekly averages with the open-face 3-stage filter pack which is mounted atop a 10-m tower to collect air pollutants in the form of gases and particles. Ozone measurements are reported each hour.

In this study, the weekly measurement of sulfur dioxide (SO_2), particulate sulfate (SO_4) and particulate nitrate (NO_3) are processed to obtain annual means at the seven selected sites geographically paired with SURFRAD sites (see Figure 1). In order to provide high quality data, the measurements were analyzed relative to data quality indicators (DQI) such as precision, accuracy and completeness and their associated metrics (CASTNET 2010 Annual Report, 2012). These analyses demonstrate that CASTNET data can be used with confidence for multi-year trend analysis. The standards and policies for all components of project operation from site selection through final data reporting are documented in the CASTNET Quality Assurance Project Plan Revision 8.0 (2011). Also, the quality assurance reports are produces four times per year with the fourth quarter report including an annual summary. The dataset and documentations can be found at http://epa.gov/castnet/javaweb/index.html.

2.4 Interagency Monitoring of Protection of Visual Environments (IMPROVE)

The IMPROVE program began in 1988 and is a cooperative measurement effort designed to establish current visibility and aerosol conditions in mandatory Class I areas (CIAs) and identify chemical species and emission sources responsible for existing anthropogenic and natural visibility impairment. This network consists of approximately 212 sites (170 on-going and 42 discontinued sites). Again, we are only interested in those sites which are in the vicinity of SURFRAD and ARM sites (see Figure 1 and Table 1).

Each monitoring approach has its own inherent limitations and biases. Determination of gravimetric mass has both negative and positive artifacts. For example, ammonium nitrate (NH_4NO_3) and other semivolatiles are lost during sampling; on the other hand, measured mass includes particle-bound water. Moreover, some species may react with atmospheric gases, which will further increase the positive mass artifact. In particular, estimating aerosol species concentrations requires assumptions concerning the chemical form of various compounds, such as nitrates, sulfates, organic material and soil composition. For example, the IMPROVE Report V (June 2011) shows that differences on the order of 20% in organic carbon (OC) mass can occur, depending on which sampling system is used. However, all these uncertainties in gravimetric and speciation measurements are considered to be within an acceptable range (Malm et al., 2011). More details regarding sites locations, instruments, aerosol sampling and analysis and uncertainties in measurements can be found in IMPROVE Report V June 2011. The data can be found at

http://vista.cira.colostate.edu/improve/Data/data.htm.

2.5 Trend Estimation

The results from each observation network are presented in all figures as time series of annual mean anomalies (except AOD is represented as annual mean) for each site together with their network mean (solid black line) of eastern US (i.e. averaging the annual mean of BON, GWN, PSU and SGP to obtain the eastern network mean) and of western US (i.e. averaging the annual mean of TBL, FPK and DRA to obtain the western network mean). Least square fits (LSF) are applied to the eastern and western network mean to determine the tendencies (dash black line). The scatter of the individual sites represents the uncertainty of the network mean and the consistency of the measurements among the various sites in a given region. To ensure the estimated trends are statistically significant, a regression analysis is used to account for autocorrelation and variability in the observed data. This statistical methodology is based on Weatherhead et al. (1998), which has been applied in many studies (Hsu et al., 2012; de Meij et al. 2012). The general principle and its application in our study are briefly discussed in the following paragraph.

After obtaining the annual mean for each dataset (i.e. SW radiation, AOD and aerosol concentration), each trend is determined as the slope coefficient (*m*) of the LSF. Assuming a simple linear model,

$$Y_t = mX_t + c + N_t \qquad (1)$$

where Y_t is the observed value at time *t*, *c* is the intercept term, *m* is the slope, X_t is year t of the time series and N_t is the noise of the time series (i.e. residual from the straight-line fit at time *t*). This noise term is assumed to be autoregressive with a lag of one time period (i.e. $N_t = \varphi N_{t-1} + \varepsilon_t$, where φ is the autocorrelation coefficient and ε_t are independent and identically distributed random variables with mean zero, and variance σ_ε^2). Once the *m* has been estimated using generalized least squares regression (i.e. $\hat{m}$), the standard deviation of $\hat{m}$ can be estimated by:

$$\sigma_m \approx \frac{\sigma_n}{t^{\frac{3}{2}}} \sqrt{\frac{1+\varphi}{1-\varphi}} \quad (2)$$

where σ_N is the standard deviation of the noise parameter N_t, and *t* is the number of years. The significance of the trend can be assessed using the ratio $\frac{|\hat{m}|}{\sigma_m}$, i.e. the absolute trend relative to its uncertainty estimate. This ratio is assumed to be approximately normally distributed with mean zero and standard deviation 1. Thus, if this ratio is 1.96 or greater, the trend is significant at the 95% confidence level. Similarly, if this ratio is greater than 1.65, the trend is significant at the 90% confidence level. In general, Table 2 shows that all trends are significant at the 95 % confidence level except the clear-sky direct SW in both eastern and western US from radiation sites and NO_3 in eastern US from IMPROVE observations are lower than 90% confidence level. Note that it becomes harder to detect a trend with a given level of confidence as σ_m increases. Unless stated otherwise, the term "significant" in this study indicates that the estimated trend is statistically significantly different from zero at the given confidence level.

3 Result and Discussion

3.1 Emission trends

Several studies (Streets et al., 2006; Smith et al., 2011; McDonald et al., 2012; Xing et al., 2012; Hand et al., 2012) show the CAA controls have successfully reduced air pollutants emissions in the US since 1990, especially SO_2 and NO_x. For instance, the SO_2 and NO_x emissions processed using the methodology described in Xing et al. (2012) show decreasing trends for each site (Figure 2 a-d). The emission data is generated with a spatial resolution of 12 km x 12 km grid cell because of the configurations for the coupled WRF-CMAQ simulation which is under testing for the same period. The emission data displayed in this figure is extracted from the single grid cell containing each monitoring site so that the equivalent network mean can be computed in the same manner as for the observational data. To obtain a more representative depiction of US emission trends, the average based on all grid cells in the west and east regions is also calculated (e.g. use longitude -100^o to separate west and east) which are identified as regional means. This is more representative because the network mean (i.e. averaging 3 grid cells co-located with SURFRAD sites for the west network and 4 grid cells co-located with SURFRAD sites for the east network) may be dominated by anomalous emission rates in these few grid cells. Also, note that concentrations at a point do not necessarily originate from emissions only at that point. For example, although the western network mean (averaging of three sites) is mostly driven by the TBL emission (shown in Figure 2 b), the overall western regional mean (averaging of western states) still demonstrate a decreasing trend in Figure 3 b. Note that, as shown in Figures 2 and 3, these emission trends, either network (SO_2 east: -0.07 μg/m^3/year, SO_2 west: -0.01 μg/m^3/year, NO_x east: -0.09 μg/m^3/year and NO_x west: -0.06 μg/m^3/year) or regional averages (SO_2 east: -0.56 Tg/year, SO_2 west: -0.16 Tg/year, NO_x east: -0.41 Tg/year and NO_x west: -0.22 Tg/year), indicate a more dramatic change in the eastern US compared to the western US. This is most likely because of the CAA controls were aimed to reduce the air pollutants emission in the eastern US where most of the electric generation units (EGUs) and other industrial facilities are located. In other words, since the SO_2 and NO_x emissions are low in the western US to begin with, the application of CAA controls did not affect pollutant emissions as drastically.

3.2 Aerosol trends

The AOD is often used as a surrogate for the tropospheric aerosol burden; consequently long-term changes in AOD can also be used to verify the trends in the tropospheric aerosol burden as well as associated trends in their optical and radiative characteristics. Therefore, one of the analyses is to examine the trends in total column AOD at the SURFRAD and ARM sites in conjunction with surface concentration measurements at the paired CASTNET and IMPROVE sites (refer to Figure 1 and Table 1).

To begin with, we investigate the cloud-screened AOD from SURFRAD and ARM together with total $PM_{2.5}$ from IMPROVE to assess the effect of reductions in anthropogenic aerosol burden resulting from substantial reductions in emissions of SO_2 and NO_x over the past 16 years across the US. First, Figure 4 a-b shows that in the eastern US there is better correlation

(R=0.71) between AOD and $PM_{2.5}$ than in the western US (R=0.58). Note that the IMPROVE sites in the western US are further from the SURFRAD sites compared to the eastern US (see Table 1 for distances). As presented in Figure 5 a-d, both trends of the cloud-screened AOD (East: -0.0012 1/year and West: 0.0009 1/year) and $PM_{2.5}$ (East: -0.30 $\mu g/m^3$/year and West: 0.02 $\mu g/m^3$/year) agree well with each other (i.e. decreasing in the eastern US while the western US demonstrates a small increasing trend). This is not surprising to because the air pollutants level is much higher in the eastern US before 1995 while the western mean AOD (less than 0.1) and $PM_{2.5}$ (less than 5 $\mu g/m^3$) are always much lower than the eastern values. Another possible contributing factor for this phenomenon at the western sites could be changes in the long range transport of aerosol / dust plumes which can cause enhancements in both surface aerosol concentrations and AOD (Gan et al., 2008; Mathur, 2008; Miller et al., 2011; Uno et al., 2011) and possibly contribute to the noted trends in both surface and aloft tropospheric aerosol burden. Also, note that these trends in the tropospheric aerosol burden are consistent with the analysis of Hsu et al. (2012) who reported large reductions in AOD over eastern US and Europe.

Analysis of trends in surface concentrations from IMPROVE (i.e. SO_4 east:-0.093 $\mu g/m^3$/year, SO_4 west: 0.004 $\mu g/m^3$/year, NO_3 east: 0.003 $\mu g/m^3$/year and NO_3 west: 0.007 $\mu g/m^3$/year) and CASTNET (i.e. SO_2 east: -0.209 $\mu g/m^3$/year, SO_2 west: -0.012 $\mu g/m^3$/year, SO_4 east: -0.135 $\mu g/m^3$/year, SO_4 west: -0.003 $\mu g/m^3$/year, NO_3 east: -0.103 $\mu g/m^3$/year and NO_3 west: -0.011 $\mu g/m^3$/year) also shows similar results (see Figure 6 and 7), except that NO_3 from CASTNET is decreasing while NO_3 from IMPROVE has a small increasing trend in both regions and SO_4 in the western US from both networks shows almost no trend. As shown in both figures, the changes in SO_2, SO_4 and NO_3 are relatively small (almost no trend) in the western US. The small difference in NO_3 between networks may be due to the locations of the measurements that may be influenced by nearby agriculture activities. The overall results indicate that the impact of the large reductions in emissions of SO_2 and NO_x resulting from a variety of control measures under the CAA and its amendments is evident in the decreasing trends in both the surface particulate matter concentrations as well as the AOD especially in the eastern US (Streets et al., 2006; Smith et al., 2011; McDonald et al., 2012; Xing et al., 2012; Hand et al., 2012). Note that the minor differences between the emission and the surface concentration trends in the western US may due to the methodology of emission processing. According to Xing et al. (2012), there are some assumptions and uncertainties in the emission data which can be caused by the lag in reporting in rural areas of the western US during the early period and changes in measurement methodologies of certain sources.

3.3 Radiation trends

The surface radiation measurements from SURFRAD and ARM are evaluated in this study since the aerosol loading in the atmosphere can have a strong effect on radiation. The change of aerosol loading and cloud cover affect the amount of solar energy that reaches the ground. In general, the SW radiation (i.e. both direct and diffuse) is mostly affected by clouds, aerosols (e.g. scattering and absorptive), atmospheric molecules and certain radiatively active gases (e.g. water vapour and ozone). Note that the contribution of Rayleigh scattering of molecules is neglected in this study because it is assumed constant over time and therefore does not affect the SW radiation trends.

First, we examined the cloud cover trends together with the all-sky downwelling, direct and diffuse SW radiation trends at these seven sites. Note that, cloud cover (also known as cloudiness or cloud amount) refers to the fraction of the sky obscured by clouds when observed from a particular location and is unitless. In Figure 8 a-d, the all-sky downwelling total (East: 0.63 W/m^2/year and West: 0.51 W/m^2/year) and direct (East: 0.41 W/m^2/year and West: 0.17 W/m^2/year) SW radiation in both regions exhibits increasing trends which indicate more solar energy reaches the ground. At the same time, the trends of all-sky diffuse (East: 0.26 W/m^2/year and West: 0.40 W/m^2/year) SW radiation (Figure 8 e-f) also increase in east and west regions while the cloud cover (East: -0.002 1/year and West -0.001 1/year) in Figure 8 g-h shows a decreasing trend. This outcome suggests that other factors besides the direct effects of aerosol loading are affecting the all-sky diffuse SW radiation. Moreover, the study of SW and LW radiation by Augustine and Dutton (2013), and SW by Long et al. (2009), suggests that the SW brightening in the US is related to a decrease in cloud coverage and aerosol direct effects may only play a smaller role in this phenomenon. However, the reduction of aerosol loading may be contributing to the decrease in cloud cover through indirect effects whereby reduced concentrations of cloud condensation nuclei (CCN) can cause reductions in cloud albedo and lifetime (Lohmann and Feichter, 2005). On the other hand, changes in atmospheric circulation patterns that may have occurred over this time period may also have contributed to the observed changes in cloud cover. For example, Augustine and Dutton (2013) mentioned that during this study period not only the greenhouse gases were affecting the surface radiation budget but the atmospheric circulation associated with ENSO (El Niño/Southern Oscillation) can also potentially dissipate the excess sensible heat from the major increase in the surface radiation. Overall, while the all-sky downwelling SW radiation is increasing, it is hard to attribute this trend to the individual or combined changes in either the aerosol loading or clouds since these measurements reflect both effects. Therefore, evaluating the clear-sky downwelling, direct and diffuse SW radiation may give us a better idea of direct aerosol effects on SW radiation as it eliminates the cloud effects.

In Figure 9, the clear-sky downwelling total SW radiation (East: 0.37 W/m^2/year and West: 0.48 W/m^2/year) is increasing in both regions of US but the clear-sky direct SW radiation (East: -0.009 W/m^2/year and West: 0.001 W/m^2/year) shows virtually no trend. Moreover, the clear-sky diffuse SW (East: 0.38 W/m^2/year and West: 0.48 W/m^2/year) also displays an increasing trend about equal to the total clear-sky SW trend. This result seems inconsistent with the analysis of AOD and surface concentration trends, particularly those in the eastern US. However, similar trends in clear-sky diffuse SW radiation were reported in the analysis of Long et al. (2009) who suggested that increasing trends at all of the sites analyzed in the present study may be indicative of radiation changes owing to processes other than the dry aerosol direct effects such as aerosol indirect/semi-indirect effects and/or the variation in the atmospheric humidity profile (e.g. increased high-altitude air traffic) that generate thin cirrus haze but are still traditionally included in the clear-sky classifications. For example, as noted by Dupont et al. (2008), an optical depth of about 0.15 or less at visible band is considered as "clear-sky" in the classification of the RFA methodology and this definition is consistent with human and sky imager observations (Long et al., 2006). Furthermore, as explained by Long et al. (2009), the AOD retrievals include a field-of-view (FOV) larger than the solar disk, such that enhanced forward scattering would be inferred as a reduction in optical depth. As a result, subvisual cirrus would lead to enhanced measurements of the clear-sky downwelling diffuse SW component while at the same time biasing the AOD retrievals low. For example, any increase in the direct due to actual decreases in aerosols can be compensate by the large mode ice crystal scattering of SW out of the direct instrument FOV into the diffuse field (Long et al., 2009). Meanwhile, these results suggest that anthropogenic aerosols are not the key factor that influences the trend in clear-sky diffuse SW in the western US because the changes in AOD and surface concentrations are relatively small (almost no trend or slightly increasing) while the trends of the clear-sky SW and clear-sky direct behave similar as those trends in eastern US.

Despite these confounding factors, the increasing trend in clear-sky downwelling SW radiation in the eastern US may be at least partially caused by the reduction of anthropogenic aerosol loading as the AOD and surface concentrations both have decreasing trends. In particular, Figure 10 a-d show an interesting finding that both AOD and $PM_{2.5}$ are decreasing in the eastern US and remain relatively stable in the western US while the clear-sky SW radiation is increasing over the past 15 years in both regions. Moreover, Xing et al. (2012) showed that the control measures under the CAA have led to substantial reductions in emissions (total SO_2 and NO_x emissions in the US decreased by roughly 65% and 50%, respectively, between 1990 and 2010), and that many of these reductions were especially pronounced in the eastern US. The anti-correlation between AOD and clear-sky downwelling SW radiation is suggestive of decreasing aerosol direct radiative effects. One of the possible causes of increasing clear-sky diffuse radiation can be the location of the sites which are close to urban regions and may be influenced by air traffic activities as shown in Figure 11 (several international and regional airports are located in this region). The contrail-generated ice haze from the associated air traffic may confound the interpretation of clear and cloudy sky at those sites in eastern US (Long et al., 2009). Also, note that the clear-sky downwelling SW radiation is estimated based on RFA (Long and Ackerman, 2000; Long and Gaustad, 2004) so there are some uncertainties in this estimation. For example, Long and Ackerman (2000) showed that the interpolated fits produced clear-sky radiation estimated with a root mean square uncertainty of ~3% which is caused by the unidentified column water vapor and aerosol changes normally occurring between clear-sky fitted days.

In order to further examine the causes of the increasing trend in clear-sky diffuse SW in the eastern US, we analyzed the US domestic airline route network from the major airlines (i.e. Continental, United, US Airways and Delta airlines). This analysis illustrated that a majority of the routes (see Figure 12 for the combined routes from US Airways and Delta airlines.) are over the eastern US with major airport hubs (see Figure 11) in urban area such as Chicago, New York City, Atlanta, and Houston which can lead to an increase in contrail-generated haze (i.e. subvisual cirrus) (http://contrailscience.com/interactive-flight-map-visualization/). Moreover, Figure 13 illustrates the total flight hours of aircraft over the US (source: US Bureau of transportation Statistics) rose notably from 1996 through 2010. The growth of aviation together with the major airline routes crossing the eastern US can potentially enhance the contrail-generated haze and this can further enhance the "clear-sky" diffuse SW measurements (Yang et al., 2010; Burkhardt et al., 2010). Also, note that during the last 3 years (2008-2010) the total flight hours are reducing while the clear-sky diffuse is also decreasing which can be one of the clues that the contrails is related to the diffuse radiation. Consequently, this finding can be one of the possible causes of the increasing clear-sky diffuse SW radiation trend since the observation sites are located close to areas with dense air traffic (see Figure 1).

4 Summary and Conclusions

The analysis conducted in this study attempts to determine the consequence of the changes in troposphere aerosol burden arising from substantial reductions in emissions of SO_2 and NO_x associated with control measures under the CAA over the past 16 years especially on trends in solar radiation. Radiation measurements for the period 1995-2010 from the SURFRAD and ARM sites in the US are analyzed in conjunction with observations of surface concentrations (CASTNET and IMPROVE) and AOD (SURFRAD) at sites in the vicinity of these radiation measurement sites. This pairing of data from various networks provides an opportunity to examine trends in aerosol burden and associated radiative effects for various sub-regions across the US and give insight into the causes of observed "brightening".

The outcome from this study suggests that emission controls (Streets et al., 2006; Smith et al., 2011; McDonald et al., 2012; Xing et al., 2012; Hand et al., 2012) resulted in a substantial reduction in aerosol burden over the North American troposphere, especially across the eastern US, and also shows an associated increase in surface solar radiation over large portions of the eastern US. However, analysis of the clear-sky diffuse SW radiation shows that the radiative impacts of decreasing aerosol concentrations are confounded by other factors. Specifically, the clear-sky diffuse SW radiation was shown to have an increasing trend at all sites, the opposite of what would be expected if changes in clear-sky radiation were solely attributable to changes in the aerosol direct effect. There are several possible interpretations to resolve this seeming contradiction. To begin with, we examined the high-altitude air traffic (spatial and temporal) over the US which can potentially enhance the cirrus haze occurances together with the procedure for the classification of "clear-sky" conditions in the radiation retrieval methodology. The analysis shows that air traffic is heaviest over many areas of the eastern US and that there has been a steady decadal growth of air traffic (Long et al. 2009). Moreover, as discussed by Long at el. (2009), the traditional classification of "clear-sky" includes some amount of condensed water in the atmosphere column, including subvisual cirrus and cirrus haze that have an influence on the clear-sky downwelling SW radiation partitioning (between the direct and diffuse components) observed at the surface. Particularly, the AOD retrievals include a FOV larger than the solar disc which can enhance the forward scattering and hence be erroneously interpreted as decreases in optical depth. At the same time, migration of a mostly dry aerosol small-mode scattering and absorption to a mix that includes a significant large mode primarily scattering component can act to offset any increase in the direct component FOV from decreasing aerosols by increased scattering into the diffuse component due to ice crystals, as detailed in Long et al. (2009). Unraveling the contributions of the various direct, semi-indirect and indirect aerosol effects as well as other cloud effects to changes in SW radiation will be pursued through the use of coupled modeling systems such as WRF-CMAQ (Wong et al., 2012) and will be the subject of future studies. Meanwhile, the causes for the increase of the clear-sky diffuse SW in the western US can be similar to the eastern US because the AOD and the surface aerosol concentrations in the western US are low since 1995 and do not vary remarkably.

In conclusion, this analysis suggest that there was a SW radiation "brightening" over the past 16 years in the US (Wild et al., 2009; Long et al., 2009). For all-sky SW radiation, the "brightening" occurs at the same time that cloudiness exhibits a decreasing trend suggesting the possibility that indirect effects of decreasing aerosols may be a contributing factor. However, association does not prove causation, especially considering that trends in cloud cover can have many other reasons. The clear-sky SW radiation may be associated at least in part with a decrease in aerosols, particularly in the eastern US where substantial reductions in anthropogenic emissions of SO_2 and NO_x, (Xing et al., 2012; Hand et al., 2012) resulting from the implementation of control measures have resulted in a decrease in the tropospheric aerosol burden. The relationship of the radiation brightening trend to aerosol decreases is less apparent at the western U.S.; this region could be influenced by local terrain influences as well as episodic long-range pollution transport which may contribute to the lack of a clear association between trends in aerosol burden and surface radiation at these locations. Nevertheless, the association of "brightening" with the aerosol direct effect is confounded by increasing trends in clear-sky diffuse SW. Thus, it seems that other factors may play a role in the increasing of clear-sky diffuse SW radiation. Moreover, the indirect aerosol and other cloud effects (Ruckstuhl et al., 2008) as well as the water vapor concentration (Haywood et al., 2011) can potentially influence the surface solar energy. Thus, more studies are needed to evaluate these factors. Furthermore, the existence of an association between trends in surface solar radiation and aerosol burden provide a unique test for the current generation of climate-chemistry models. Multi-decadal model calculations with the coupled WRF-CMAQ model (Wong et al., 2012) are being performed for the 1990-2010 period to test the ability of the model to simulate not only the changes in aerosol burden over the US arising from the implementation of the CAA, but also the associated radiation brightening as analyzed in the present analysis. Results from these modeling studies and their comparison with the trends inferred from the observations will be reported in subsequent contributions.

Acknowledgements

This research was performed while Chuen-Meei Gan held a National Research Council Research Associateship Award at US EPA. The research presented in this study was supported through an interagency agreement between the US Department of Energy (funding IA DE-SC0003782) and the US Environmental Protection Agency (funding IA RW-89-9233260). It has been subject to the US EPA's administrative review and approved for publication. The author also would like thank John Augustine from NOAA-SURFRAD for his support and assistance in obtaining the SURFRAD data. Dr. Long acknowledges the support of the Climate Change Research Division of the US Department of Energy as part of the Atmospheric System Research (ASR) Program. We also appreciate the comments of three reviewers that have significantly improved this paper.

References

Augustine, J. A., DeLuisi, J. J. and Long, C. N.: SURFRAD – A national surface radiation budget network for atmospheric research, Bull. Am. Meteorol. Soc., 81(10), 2341 – 2357, doi:10.1175/1520- 477(2000)081<2341:SANSRB>2.3.CO;2, 2000.

Augustine, J. A., Hodges, G. B., Cornwall, C. R., Michalsky, J. J. and Medina, C. I.: An update on SURFRAD—The GCOS surface radiation budget network for the continental United States, J. Atmos. Oceanic Technol., 22, 1460– 1472, doi:10.1175/JTECH1806.1, 2005.

Augustine, J. A., Hodges, G. B., Dutton, E. G., Michalsky, J. J. and Cornwall, C. R.: An aerosol optical depth climatology for NOAA's national surface radiation budget network (SURFRAD), J. Geophys. Res., 113, D11204, doi:10.1029/2007JD009504, 2008.

Augustine, J. A. and Dutton, E. G.: Variability of the surface radiation budget over the United States from 1996 through 2011 from high-quality measurements, J. Geophys. Res. Atmos., 118, 43-53, doi:10.1029/2012JD018551,2013.

Burkhardt, U., Kärcher, B. and Schumann, U.: Global modeling of the contrail and contrail cirrus climate impact, AMS BAMS, doi: 10.1175/2009BAMS2656.1, April 2010

CASTNET 2010 Annual Report.: (available at http://java.epa.gov/castnet/documents.do), April 2012.

CASTNET Quality Assurance Project Plan Revision 8.: (available at http://java.epa.gov/castnet/documents.do), October 2011.

de Meij, A., Pozzer, A. and Leilieveld, J.: Trend analysis in aerosol optical depths and pollutant emission estimates between 2000 and 2009, Atmos. Environ., 51, 75–86, doi:10.1016/j.atmosenv.2012.01.059, 2012.

Dupont J.C., Haeffelin, M. and Long, C.N.: Evaluation of cloudless-sky periods detected by shortwave and longwave algorithms using lidar measurements, GRL 35(10), doi:10.1029/2008GL033658, 2008.

Dutton, E. G., Nelson, D. W., Stone, R. S., Longenecker, D., Carbaugh, G., Harris, J. M. and Wendell, J.: Decadal variations in surface solar irradiance as observed in a globally remote network, J. Geophys. Res., 111, D19101, doi:10.1029/2005JD006901, 2006.

Gan, C.M., Gross, B., Moshary, F. and Ahmed, S.: Analysis of the Interaction of Aerosol Transport Layers on Local Air Quality, IGARSS 2008.

Gilgen, H., Wild, M. and Ohmura, A.: Means and trends of shortwave irradiance at the surface estimated from GEBA, J. Clim., 11, 2042–2061, 1998.

Hand, J. L., Schichtel, B. A., Malm, W. C. and Pitchford, M. L.: Particulate sulfate ion concentration and SO2 emission trends in the United States from the early 1990s through 2010, Atmos. Chem. Phys., 12, 10353–10365, 2012.

Harrison, L., Michalsky, J. and Berndt, J.: Automated multifilter rotating shadow-band radiometer: An instrument for optical depth and radiation measurements, Appl. Opt., 33, 5118– 5125, 1994.

Haywood, J. M., Bellouin, N., Jones, A., Boucher, O., Wild, M. and Shine, K. P.: The roles of aerosol, water vapor and cloud in future global dimming/brightening, J. Geophys. Res. 116, D20203, doi:10.1029/2011JD016000, 2011.

Hsu, N.C., Gautam, R., Sayer, A. M., Bettenhausen, C., Li, C., Jeong, M. J., Tsay, S.-C. and Holben, B. N.: Global and regional trends of aerosol optical depth over land and ocean using SeaWiFS measurements from 1997 to 2010, Armos. Chem Phys., 12, 8037-8053, 2012.

IMPROVE Spatial and Seasonal Patterns and Temporal Variability of Haze and its Constituents in the United States: Report V June 2011 (available at http://vista.cira.colostate.edu/improve/Publications/Reports/2011/2011.htm), 2011.

Malm, W. C., Schichteland, B. A. and Pitchford, M. L.: Chapter 8. Uncertainties in PM2.5 Gravimetric and Speciation Measurements of IMPROVE Annual Report, 2011.

Mathur, R.: Estimating the impact of the 2004 Alaskan forest fires on episodic particulate matter pollution over the eastern United States through assimilation of satellite derived aerosol optical depths in a regional air quality model, J. Geophys. Res., 113, D17302, doi:10.1029/2007JD009767, 2008.

McDonald, B. C., Dallmann, T. R., Martin, E. W. and Harley, R. A.: Long-term trends in nitrogen oxide emissions from motor vehicles at national, state, and air basin scales, J. Geophys. Res., 117, D00V18, doi:10.1029/2012JD018304, 2012.

Miller, D. J., Sun, K., Zondlo, M. A., Kanter, D., Dubovik, O., Welton, E. J., Winker, D. M. and Ginoux, P.: Assessing boreal forest fire smoke aerosol impacts on US air quality: A case study using multiple data sets, J. Geophys. Res.,116, D22209, doi:10.1029/2011JD016170, 2011.

Liepert, B. G.: Observed reductions of surface solar radiation at sites in the United States and worldwide from 1961 to 1990, Geophys. Res. Lett., 29(10), 1421, doi:10.1029/2002GL014910, 2002.

Lohmann, U. and Feichter, J.: Global indirect aerosol effects: a review, Atmos. Chem. Phys., 5, 715-737, 2005.

Long, C. N., and Ackerman, T. P.: Identification of clear skies from broadband pyranometer measurements and calculation of downwelling shortwave cloud effects, J. Geophys. Res., 105(D12), 15,609–15,626, doi:10.1029/2000JD900077, 2000.

Long, C. N., and Gaustad, K. L.: The shortwave (SW) clear-sky detection and fitting algorithm: Algorithm operational details and explanations, ARM TR-004, 26 pp., U. S. Dep. of Energy, Washington, D. C. (available at http://science.arm.gov/vaps/swflux.stm), 2004.

Long, C. N., Ackerman, T. P., Gaustad, K. L. and Cole, J. N. S.: Estimation of fractional sky cover from broadband shortwave radiometer measurements, J. Geophys. Res., 111, D11204, doi:10.1029/ 2005JD006475, 2006.

Long, C. N., and Shi, Y. :An automated quality assessment and control algorithm for surface radiation measurements, Open Atmos. Sci. J., 2, 23– 37, doi:10.2174/1874282300802010023, 2008.

Long, C. N., Dutton, E. G., Augustine, J. A., Wiscombe, W., Wild, M., McFarlane, S. A. and Flynn, C. J.: Significant decadal brightening of downwelling shortwave in the continental United States, J. Geophys. Res., 114, D00D06, doi:10.1029/2008JD011263, 2009.

Ohmura, A., and Lang, H. : Secular variation of global radiation over Europe, in Current Problems in Atmospheric Radiation, edited by J. Lenoble and J. F. Geleyn, pp. 98–301, A. Deepak, Hampton, Va, 1989.

Peppler, R. A., et al.: Quality Assurance of ARM Program Climate Research Facility Data, DOE/SC-ARM/TR-082, 65 pp., Dep. of Energy, Washington, D. C. (available at http://www.arm.gov/publications/tech_reports/doe-sc-arm-tr-082.pdf), 2008.

Pinker, R. T., Zhang, B. and Dutton, E. G.: Do satellites detect trends in surface solar radiation?, Science, 308, 850– 854, 2005.

Ruckstuhl, C., et al.: Aerosol and cloud effects on solar brightening and the recent rapid warming, Geophys. Res. Lett., 35, L12708, doi:10.1029/2008GL034228, 2008.

Smith, S. J., van Aardenne, J., Klimont, Z., Andres, R. J., Volke, A. and Delgado Arias, S.: Anthropogenic sulfur dioxide emissions: 1850—2005, Atmos. Chem. Phys., 11, 1101–1116, doi:10.5194/acp-11-1101-2011, 2011.

Stanhill, G., and Cohen, S.: Global dimming: A review of the evidence for a widespread and significant reduction in global radiation, Agric. For. Meteorol., 107, 255 – 278, doi:10.1016/S0168-1923(00) 00241-0, 2001.

Stoffel, T., 2005: Solar Infrared Radiation Station (SIRS) handbook. DOE Tech. Rep. ARM TR-025, 29 pp. [Available online at http://www.wmo.int/pages/prog/gcos/documents/gruanmanuals/Z_instruments/sirs_handbook.pdf.]

Streets, D. G., Wu, Y. and Chin, M.: Two-decadal aerosol trends as a likely explanation of the global dimming / brightening transition, Geophys. Res. Lett., 33, L15806, doi:10.1029/2006GL026471, 2006.

Uno, I, Eguchi, K., Yumimoto, K., Liu, Z., Hara, Y., Sugimoto, N., Shimizu, A. and Takemura, T.: Large Asian dust layers continuously reached North America in April 2010. Atmos. Chem. Phys., 11, 7333–7341, doi:10.5194/acp-11-7333-2011, 2011.

Weatherhead, E. C., Reinsel, G. C., Tiao, G. C., Meng, X.-L., Choi, D., Cheang, W.-K., Keller, T., DeLuisi, J., Wuebbles, D. J., Kerr, J. B., Miller, A. J., Oltmans, S. J. and Frederick, J. E.: Factors affecting the detection of trends: Statistical considerations and applications to environmental data, J. Geophys. Res., 103, 17149–17161, doi:10.1029/98JD00995, 1998.

Wild, M., Ohmura, A., Gilgen, H. and Rosenfeld, D.:On the consistency of trends in radiation and temperature records and implications for the global hydrological cycle, Geophys. Res. Lett., 31, L11201, doi:10.1029/2003GL019188, 2004.

Wild, M., Gilgen, H., Roesch, A., Ohmura, A., Long, C. N., Dutton, E. G., Forgan, B., Kallis, A., Russak, V. and Tsvetkov, A.: From dimming to brightening: Decadal changes in surface solar radiation, Science, 308, 847– 850, doi:10.1126/science.1103215, 2005.

Wild, M., Tru¨ssel, B., Ohmura, A., Long, C. N., Ko¨nig-Langlo, G., Dutton, E. G. and Tsvetkov, A.: Global dimming and brightening: An update beyond 2000, J. Geophys. Res., 114, D00D13, doi:10.1029/2008JD011382, 2009.

Wild, M.: Global dimming and brightening: A review, J. Geophys. Res., 114, D00D16, doi:10.1029/2008JD011470. 2009.

Wong, D. C., Pleim, J. E., Mathur, R., Binkowski, F. S., Otte, T. L., Gilliam, R. C., Pouliot, G., Xiu, A., Young, J. O. and Kang, D.: WRF-CMAQ Two-way Coupled System with Aerosol Feedback: Software Development and Preliminary Results. Geoscientific Model Development. Copernicus Publications, Katlenburg-Lindau, Germany, 5(2):299-312, 2012.

Xing, J., Pleim, J., Mathur, R., Pouliot, G., Hogrefe, C., Gan, C.-M. and Wei, C.: Historical gaseous and primary aerosol emissions in the United States from 1990–2010, Atmos. Chem. Phys. Discuss., 12, 30327-30369, doi:10.5194/acpd-12-30327-2012, 2012.

Yang, P., Hong, G., Dessler, A. E., Ou, S. S. C., Liou, K-N., Minnis, P. and Harshvardhan, Contrails and induced cirrus Optics and radiatrion. AMS BAMS. doi: 10.1175/2009BAMS2837.1, April 2010.

Table 1: Listing of site identification of each site for different networks and their measurement period which are used in this study. Distance means the approximate distance between SURFRAD/ARM sites with CASTNET or IMPROVE sites.

SURFRAD / ARM	SW Radiation	AOD	CASTNET	Aerosol Concentration	IMPROVE	Aerosol Concentration
PSU [Penn State, PA] Elevation: 0.38 km Lat : 40.72^{o} Lon : -77.93^{o}	1999-2010	1999-2009	PSU106 [Penn State, PA] Distance: 0 km Elevation : 0.38 km Lat : 40.72^{o} Lon : -77.93^{o}	1990-2010	WASH1 [Washington DC] Distance: 210 km Elevation : 0.02 km Lat : 38.88^{o} Lon : -77.03^{o}	1990-2010
BON [Bondville, IL] Elevation : 0.23 km Lat : 40.05^{o} Lon : -88.37^{o}	1995-2010	1997-2010	BVL130 [Bondville, IL] Distance: 0 km Elevation : 0.21 km Lat : 40.05^{o} Lon : -88.37^{o}	1990-2010	BONL1 [Bondville, IL] Distance: 0 km Elevation : 0.21 km Lat : 40.05^{o} Lon : -88.37^{o}	2001-2010
GWN [Goodwin Creek, MS] Elevation: 0.1 km Lat : 34.25^{o} Lon : -89.87^{o}	1995-2010	1997-2010	CVL151 [Coffeeville, MS] Distance: 30 km Elevation : 0.1 km Lat : 34.00^{o} Lon : -89.80^{o}	1990-2010	MACA1 [Mammoth Cave NP, KY] Distance: 500 km Elevation : 0.25 km Lat : 37.13^{o} Lon : -86.15^{o}	1992-2010
SGP [South Great Plain, OK] Elevation: 0.31 km Lat : 36.80^{o} Lon : -97.50^{o}	1997-2010	1996-2007	CHE185 [Cherokee, OK] Distance: 270 km Elevation : 0.3 km Lat : 35.75^{o} Lon : -94.67^{o}	2002-2010	CHER1 [Cherokee Nation, OK] Distance: 50 km Elevation : 0.34 km Lat : 36.93^{o} Lon : -97.02^{o}	2003-2010
FPK [Fort Peck, MT] Elevation: 0.63 km Lat : 48.31^{o} Lon : -105.10^{o}	1996-2010	1997-2010	THR422 [Theodore, ND] Distance: 170 km Elevation : 0.85 km Lat : 46.89^{o} Lon : -103.38^{o}	1998-2010	MELA1 [Midicine Lake, MT] Distance: 50 km Elevation : 0.61 km Lat : 48.49^{o} Lon : -104.48^{o}	2000-2010
TBL [Table Mountain, CO] Elevation: 1.69 km Lat : 40.13^{o} Lon : -105.24^{o}	1996-2010	1997-2010	ROM406 [Rocky Mtn NP, CO] Distance: 30 km Elevation : 2.7 km Lat : 40.28^{o} Lon : -105.55^{o}	1994-2010	ROMO1 [Rocky Mountain NP, CO] Distance: 30 km Elevation : 2.8 km Lat : 40.28^{o} Lon : -105.55^{o}	1991-2008
DRA [Desert Rock, NV] Elevation: 1.01 km Lat : 36.63^{o} Lon : -116.02^{o}	1999-2010	1999-2010	DEV412 [Death Valley, CA] Distance: 85 km Elevation : 0.12 km Lat : 36.51^{o} Lon : -116.85^{o}	1995-2007	DEVA1 [Death Valley NP, CA] Distance: 85 km Elevation : 0.13 km Lat : 36.51^{o} Lon : -116.85^{o}	2000-2010

Table 2: Trends (slope) for each dataset between periods of 1995 to 2010, along with the standard error and confidence level, respectively.

	Trend	**Std. Error**	$\frac{\lvert\hat{m}\rvert}{\sigma_m}$	**Confidence Level (%)**
Emission Region Mean				
SO_2 east	-0.5637	0.0129	43.68	>95
SO_2 west	-0.1643	0.0037	44.19	>95
NO_x east	-0.4086	0.0226	18.04	>95
NO_x west	-0.2231	0.0168	13.32	>95
Emission Network Mean				
SO_2 east	-0.0734	0.0030	24.88	>95
SO_2 west	-0.0108	0.0004	28.18	>95
NO_x east	-0.0918	0.0015	60.03	>95
NO_x west	-0.0617	0.0030	20.56	>95
SURFRAD and ARM				
AOD east	-0.0012	0.0003	4.26	>95
AOD west	0.0009	0.0001	6.70	>95
All-sky SW down east	0.6296	0.0566	11.13	>95
All-sky SW down west	0.5131	0.0359	14.28	>95
Clear-sky SW down east	0.3691	0.0292	12.65	>95
Clear-sky SW down west	0.4799	0.0443	10.82	>95
All-sky direct SW east	0.4149	0.0576	7.21	>95
All-sky direct SW west	0.1739	0.0488	3.56	>95
Clear-sky direct SW east	-0.0085	0.0315	0.27	<90
Clear-sky direct SW west	0.0005	0.0331	0.015	<90
All-sky diffuse SW east	0.2555	0.0235	10.86	>95
All-sky diffuse SW west	0.4009	0.0489	8.21	>95
Clear-sky diffuse SW east	0.3764	0.0107	35.11	>95
Clear-sky diffuse SW west	0.4781	0.0253	18.88	>95

Cloud cover east	-0.0021	0.0003	6.13	>95
Cloud cover west	-0.0012	0.0004	2.71	>95
IMPROVE				
$PM_{2.5}$ east	-0.2998	0.0114	26.34	>95
$PM_{2.5}$ west	0.0181	0.0074	2.44	>95
SO_4 east	-0.0933	0.0071	13.10	>95
SO_4 west	0.0038	0.0009	4.39	>95
NO_3 east	0.0025	0.0065	0.39	<90
NO_3 west	0.0069	0.0013	5.37	>95
CASTNET				
SO_2 east	-0.2089	0.0107	19.48	>95
SO_2 west	-0.0121	0.0012	10.31	>95
SO_4 east	-0.1346	0.0056	23.87	>95
SO_4 west	-0.0026	0.0010	2.53	>95
NO_3 east	-0.1026	0.0034	30.43	>95
NO_3west	-0.0110	0.0010	10.79	>95

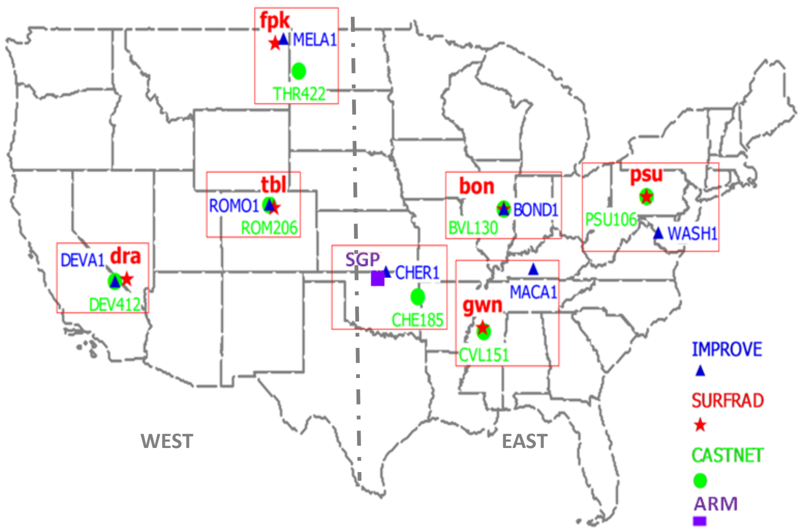

Figure 1: Locations of various sites in SURFRAD, ARM, CASTNET and IMPROVE networks.

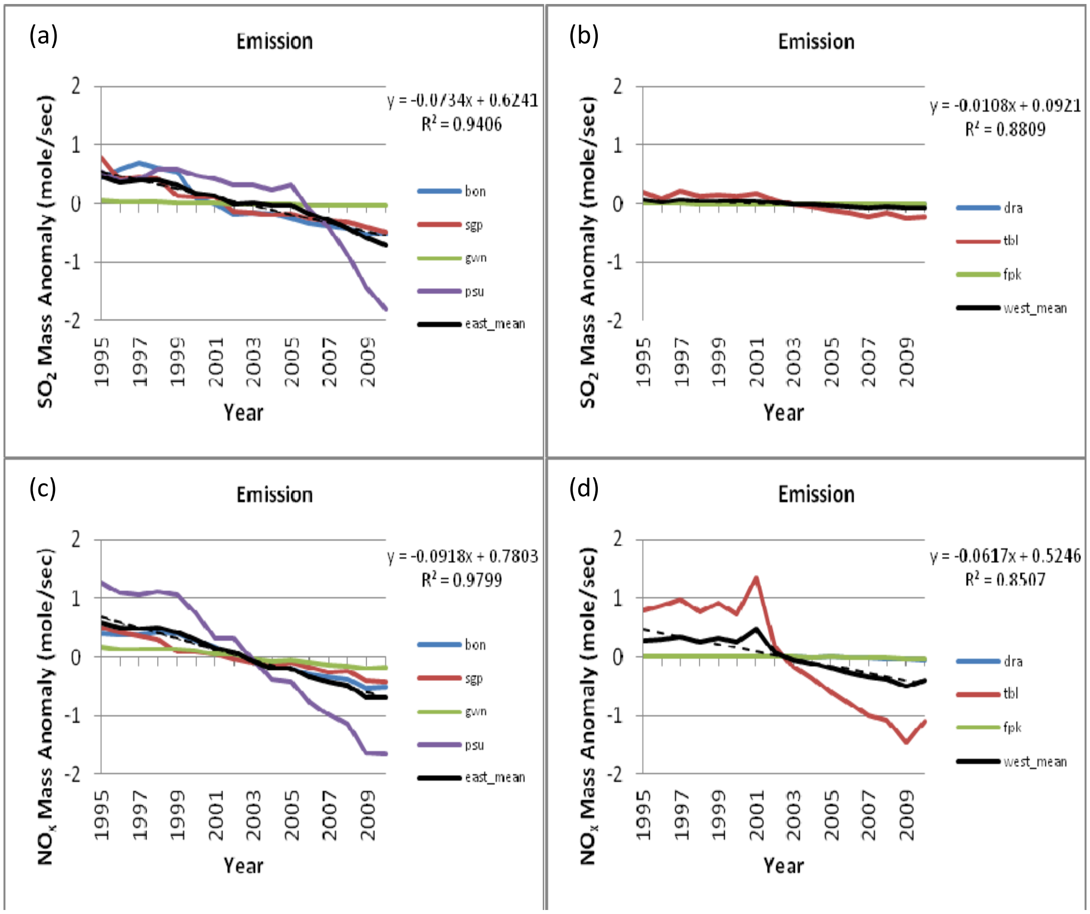

Figure 2: Annual anomalies of SO_2 (first row) and NO_x (second row) emission for each site (colored line) and the network mean (solid black line) together with the LSF (dash black line) to the network mean. The best-fit equation and coefficient of determination (R^2) are given at right in each panel. The left column represent eastern US while the right column represent western US

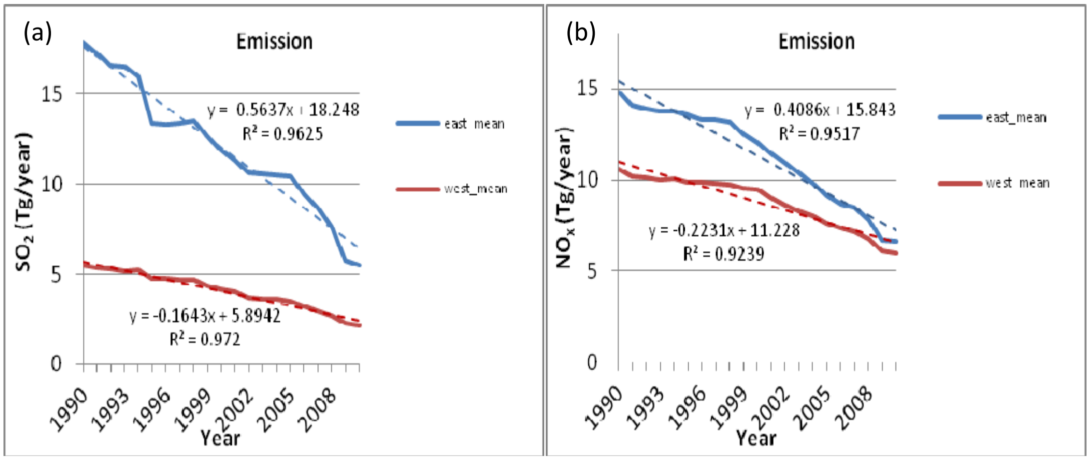

Figure 3: Annual anomalies of SO_2 (left) and NO_x (right) emission for each regional mean (solid colored line) together with their LSF (dash line). The best-fit equation and coefficient of determination (R^2) are given at right in each panel.

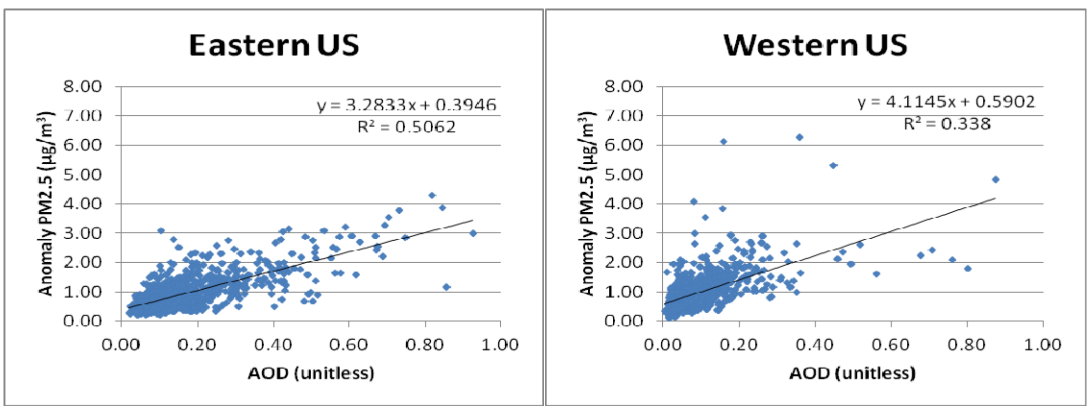

Figure 4: Scatter plot for AOD versus anomaly $PM_{2.5}$. Left panel is for eastern US and right panel is for western US. The best-fit equation and coefficient of determination (R^2) are given at right in each panel.

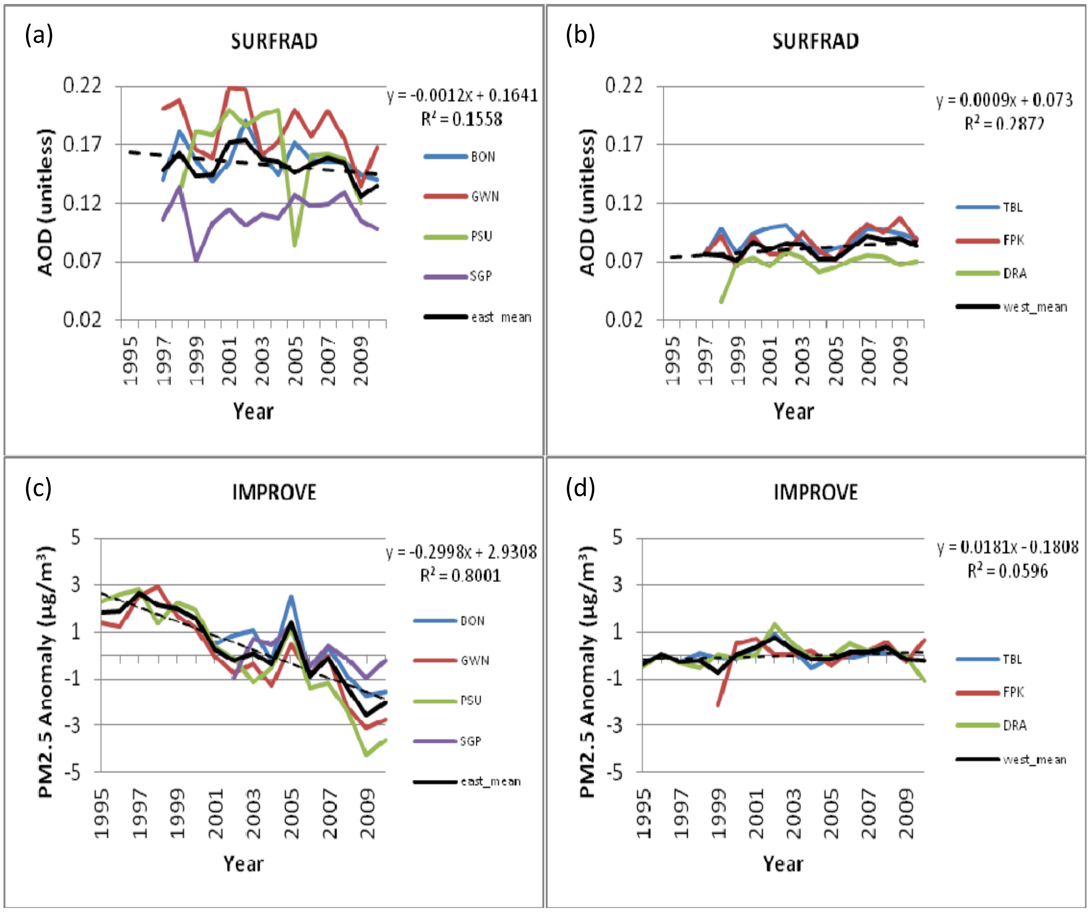

Figure 5: Annual anomalies of AOD from SURFRAD (first row) and $PM_{2.5}$ from IMPROVE (second row) for each site (colored line) and the network mean (solid black line) together with the LSF (dash black line) to the network mean. The best-fit equation and coefficient of determination (R^2) are given at right in each panel. The left column represent eastern US while the right column represent western US

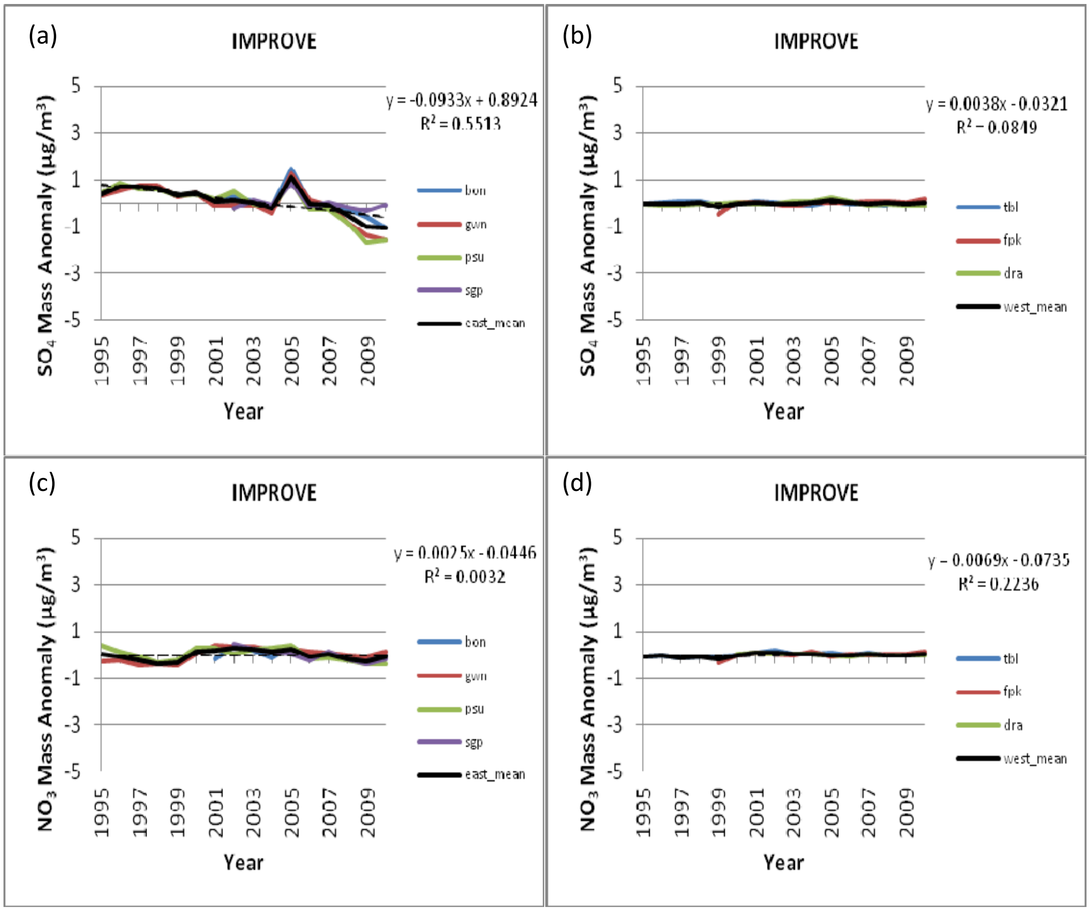

Figure 6: Annual anomalies of SO_4 (first row) and NO_3 (second row) from IMPROVE for each site (colored line) and the network mean (solid black line) together with the LSF (dash black line) to the network mean. The best-fit equation and coefficient of determination (R^2) are given at right in each panel. The left column represent eastern US while the right column represent western US

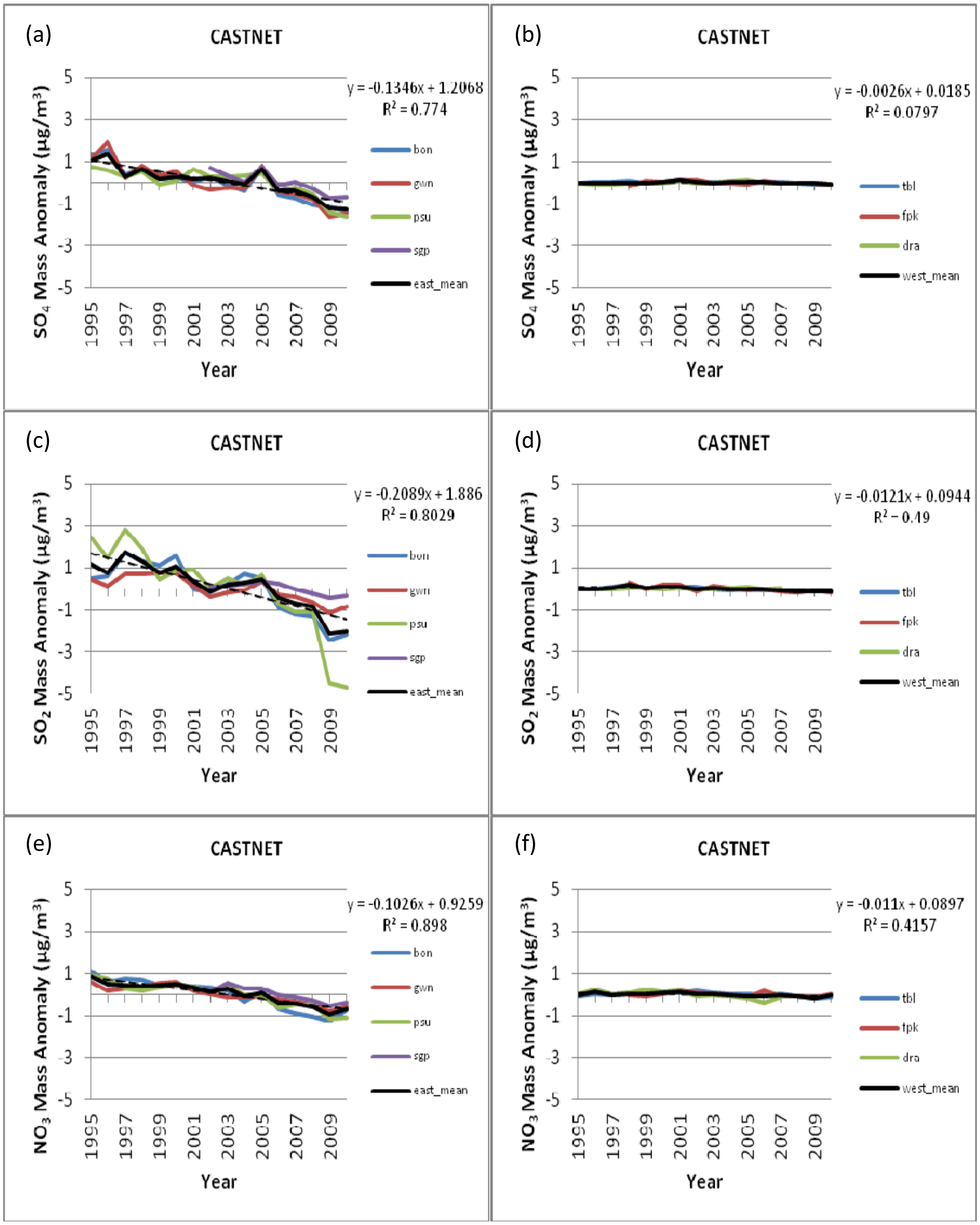

Figure 7: Annual anomalies of SO_4 (first row), SO_2 (second row) and NO_3 (third row) from CASTNET for each site (colored line) and the network mean (solid black line) together with the LSF (dash black line) to the network mean. The best-fit equation and coefficient of determination (R^2) are given at right in each panel. The left column represent eastern US while the right column represent western US

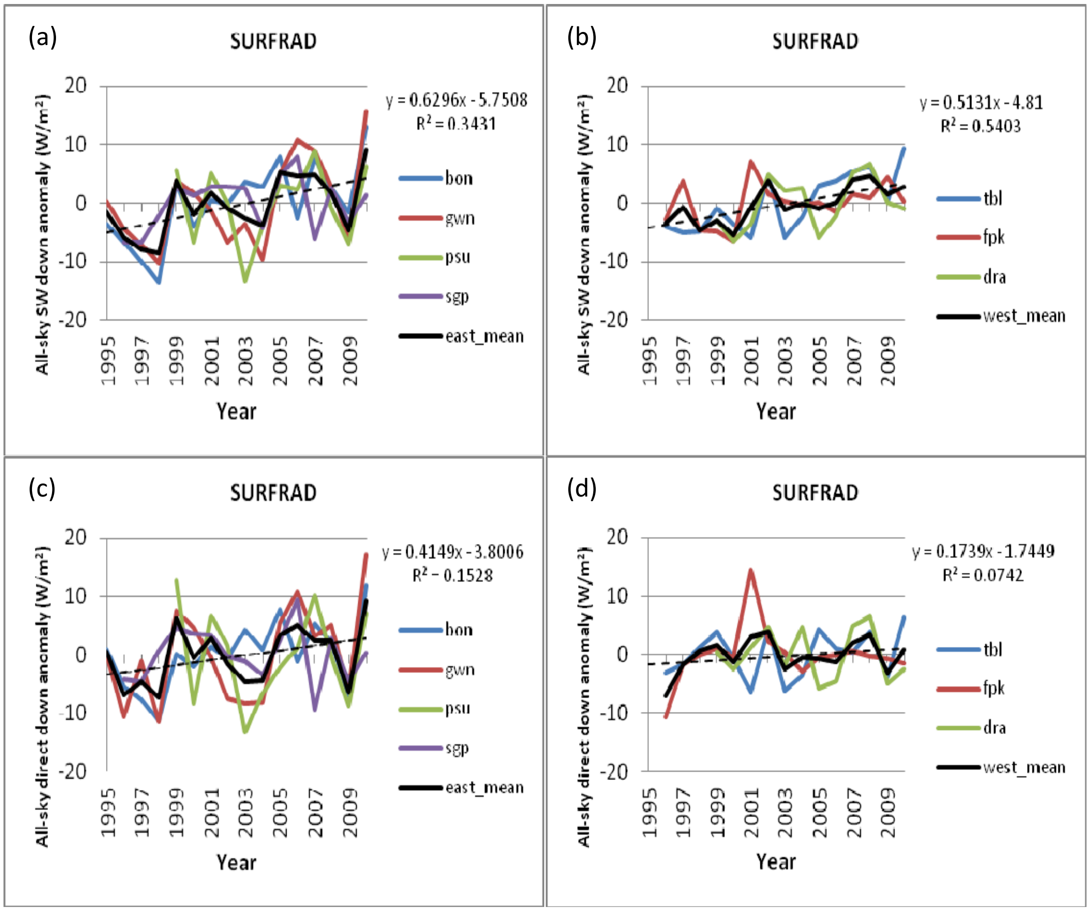
(a)
SURFRAD
All-sky SW down anomaly (W/m²)
y = 0.6296x - 5.7508
R² = 0.3431
bon
gwn
psu
sgp
east_mean
Year
(b)
SURFRAD
All-sky SW down anomaly (W/m²)
y = 0.5131x - 4.81
R² = 0.5403
tbl
fpk
dra
west_mean
Year
(c)
SURFRAD
All-sky direct down anomaly (W/m²)
y = 0.4149x - 3.8006
R² = 0.1528
bon
gwn
psu
sgp
east_mean
Year
(d)
SURFRAD
All-sky direct down anomaly (W/m²)
y = 0.1739x - 1.7449
R² = 0.0742
tbl
fpk
dra
west_mean
Year

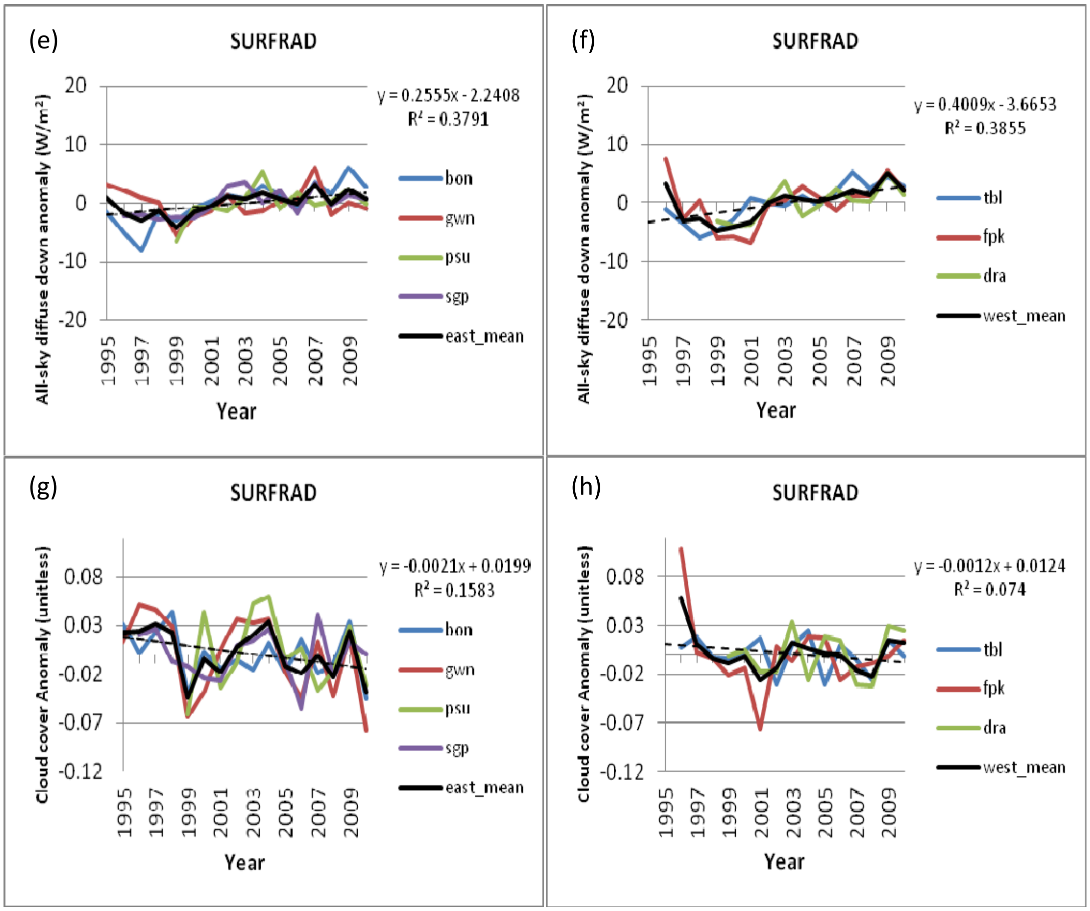

Figure 8: Annual anomalies of all-sky downwelling SW (first row), direct SW (second row), diffuse SW (third row) and cloud cover fraction(fourth row) from SURFRAD for each site (colored line) and the network mean (solid black line) together with the LSF (dash black line) to the network mean. The best-fit equation and coefficient of determination (R^2) are given at right in each panel. The left column represent eastern US while the right column represent western US

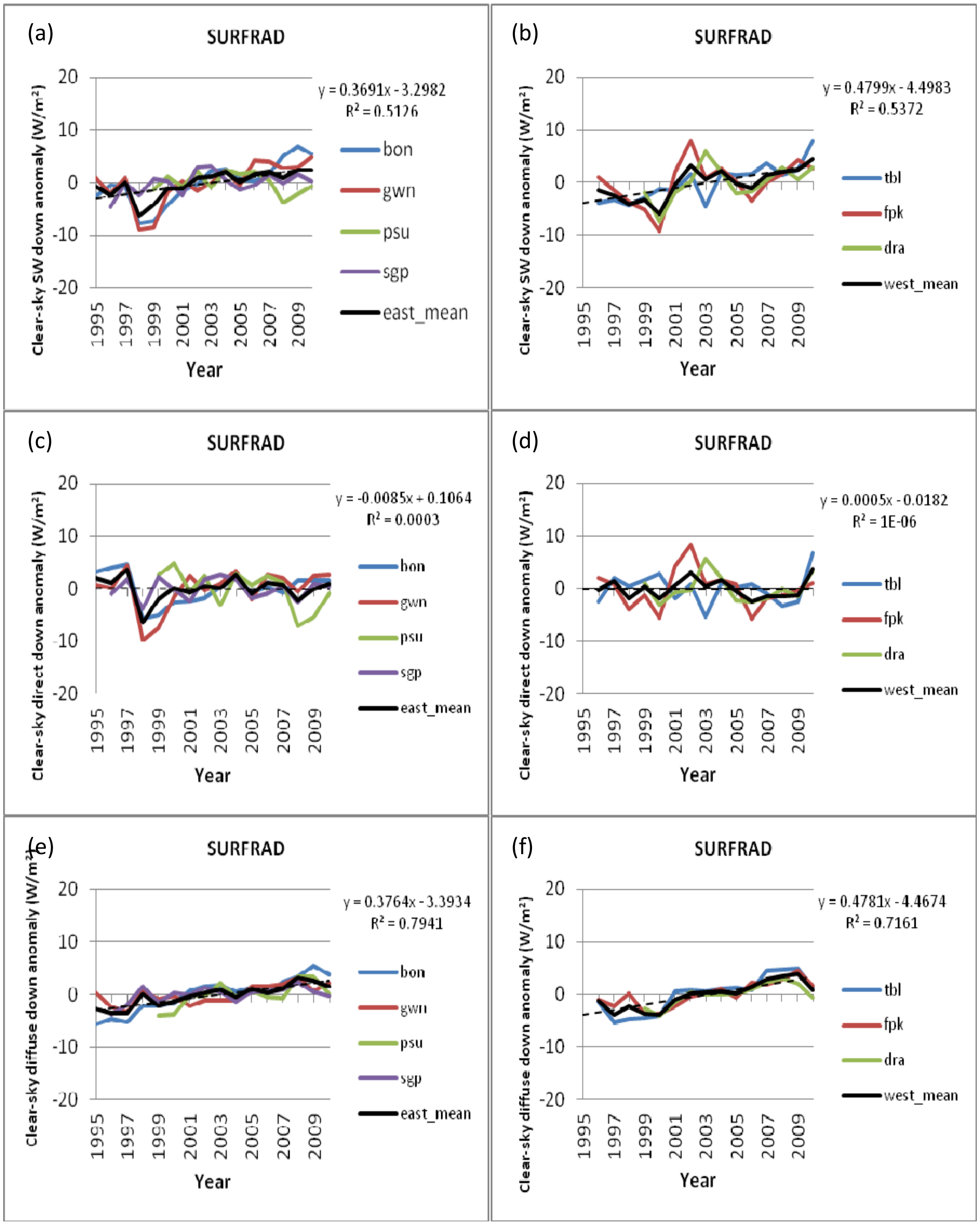

Figure 9: Annual anomalies of clear-sky downwelling SW (first row), direct SW (second row) and diffuse SW (third row) from SURFRAD for each site (colored line) and the network mean (solid black line) together with the LSF (dash black line) to the network mean. The best-fit equation and coefficient of determination (R^2) are given at right in each panel. The left column represent eastern US while the right column represent western US

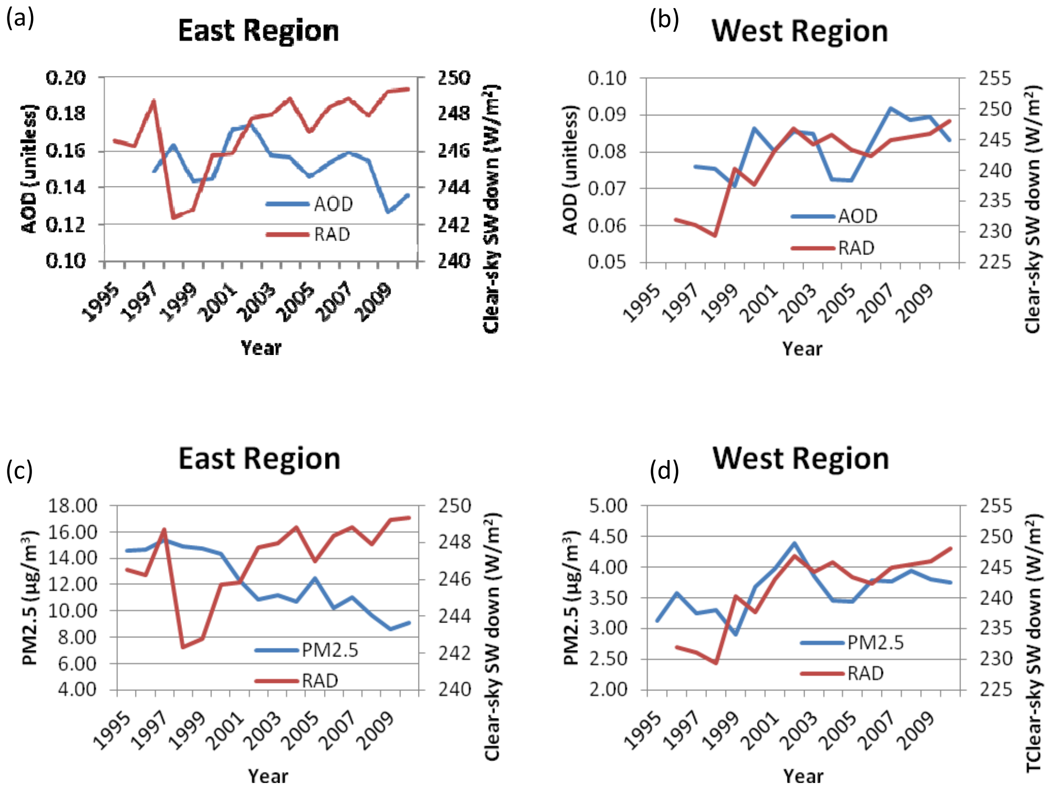

Figure 10: Panel (a-b) represent annual mean of AOD versus clear-sky SW radiation from 1995 through 2010. Panel (c-d) represent annual mean of $PM_{2.5}$ versus clear-sky SW radiation from 1995 through 2010. Left side is for east region while right side is for west region.

Figure 11: Air Traffic Hubs in US

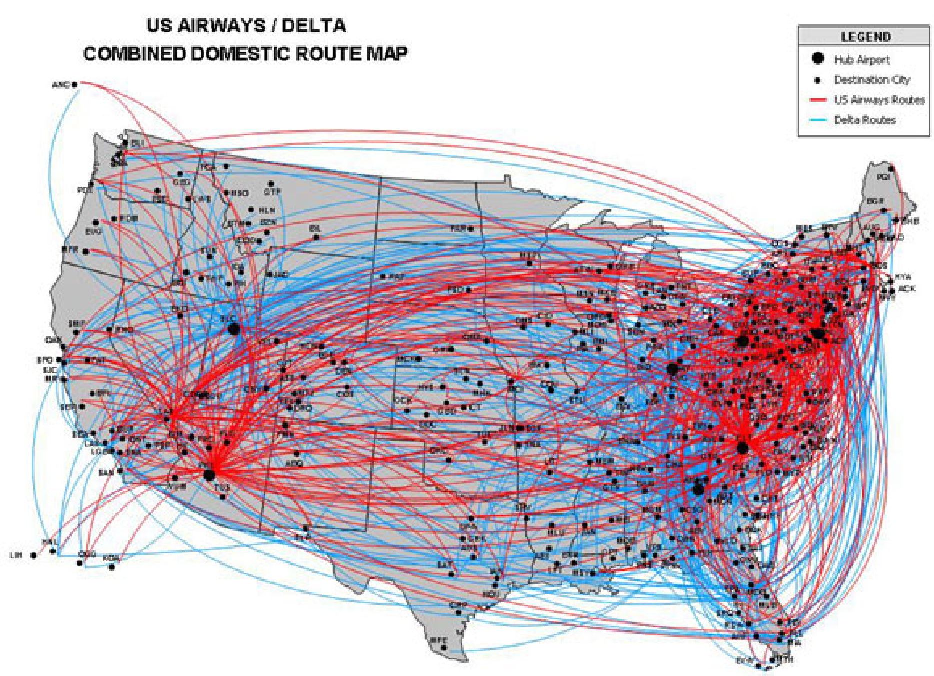

Figure 12: US Airways and Delta combined domestic routes.

(source: http://www.proaerobusiness.com/route_maps.htm)

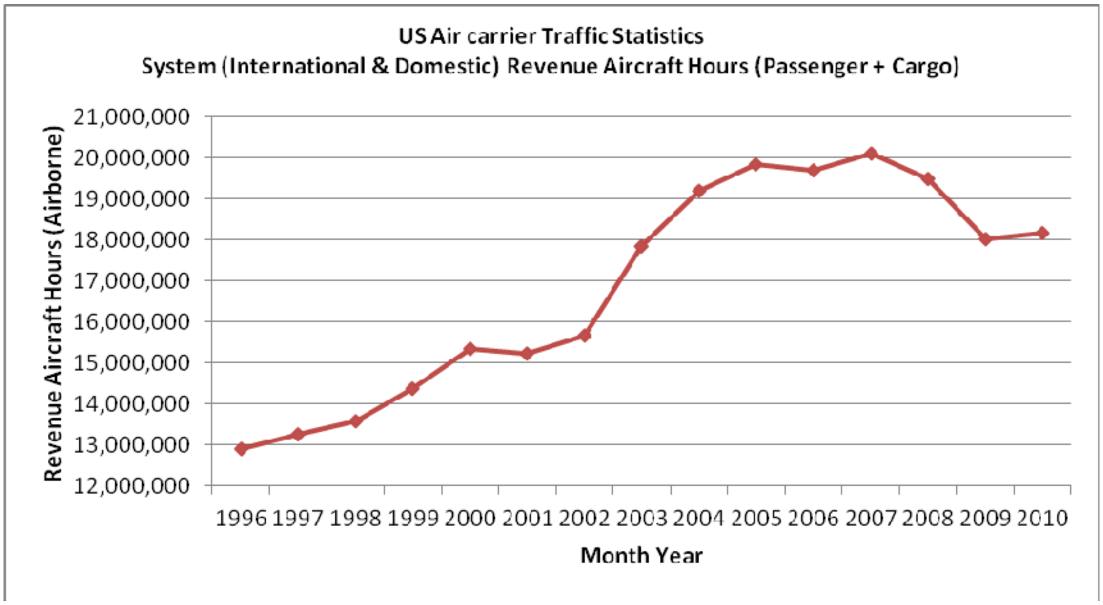

Figure 13: Monthly US system (international and domestic) aircraft airborne flight hours for the period January 1996 through December 2010 for the sum of passenger and cargo flights. (source: US Bureau of transportation Statistics)